Cellular/Molecular

c-Kit Receptor Maintains Sensory Axon Innervation of the Skin through Src Family Kinases

Adam M. Tuttle,[1] Matthew B. Pomaville,[1,2] Katherine C. Delgado,[1] Kevin M. Wright,[2] and Alex V. Nechiporuk[1]

[1]Department of Cell, Developmental, and Cancer Biology, Oregon Health and Science University, Portland, Oregon 97239, and [2]Vollum Institute, Oregon Health and Science University, Portland, Oregon 97239

Peripheral somatosensory neurons innervate the skin and sense the environment. Whereas many studies focus on initial axon outgrowth and pathfinding, how signaling pathways contribute to maintenance of the established axon arbors and terminals within the skin is largely unknown. This question is particularly relevant to the many types of neuropathies that affect mature neuronal arbors. We show that a receptor tyrosine kinase (RTK), c-Kit, contributes to maintenance, but not initial development, of cutaneous axons in the larval zebrafish before sex determination. Downregulation of Kit signaling rapidly induced retraction of established axon terminals in the skin and a reduction in axonal density. Conversely, misexpression of c-Kit ligand in the skin in larval zebrafish induced increases in local sensory axon density, suggesting an important role for Kit signaling in cutaneous axon maintenance. We found Src family kinases (SFKs) act directly downstream to mediate Kit's role in regulating cutaneous axon density. Our data demonstrate a requirement for skin-to-axon signaling to maintain axonal networks and elucidate novel roles for Kit and SFK signaling in this context. This Kit-SFK signaling axis offers a potential pathway to therapeutically target in sensory neuropathies and to further explore in other neurobiological processes.

Key words: **c-kit; multikinase inhibitor; sensory axons; skin innervation; Src; zebrafish**

Significance Statement

The skin is full of small nerve endings that sense different environmental stimuli. How these nerve endings grow and reach a specific area of the skin during development has been the focus of many studies. In contrast, the cellular and molecular mechanisms required to maintain the function and health of these structures is relatively unknown. We discovered that a specific receptor in sensory neurons, c-Kit, is required to maintain the density of nerve endings in the skin. Furthermore, we found that a molecular target of c-Kit, Src family kinases (SFKs), is necessary for this role. Thus, c-Kit/SFK signaling regulates density and maintenance of sensory nerve endings in the skin and may have important roles in neural disease and regeneration.

Introduction

Axonal growth and subsequent circuit formation require active coordination of multiple cell biological processes, many of which are well-studied (Cioni et al., 2018; Mariano et al., 2018). However, the nature of signaling pathways that promote axon maintenance is less well understood. This is particularly true of vertebrate somatosensory neurons that innervate the skin with elaborate networks of thin axonal arbors and terminals. To what extent communication between the skin and these axons contributes to this signaling and which signaling pathways are required to maintain these intricate networks is unknown.

To address this question, we employ zebrafish larvae as a model because it is amenable to high-throughput drug delivery, exquisite imaging access, and genetic interrogation. Larval zebrafish use unmyelinated Rohon–Beard (RBs) neurons for somatosensation in the trunk skin. These neurons are homologous in function and expression profile to the small-fiber neurons of the dorsal root ganglia (DRG) somatosensory neurons in other vertebrates (Faucherre et al., 2013; Palanca et al., 2013; Ogino and Hirata, 2018). By 48 h postfertilization (hpf), RB sensory neurons are functional and their axon arbors fully innervate the larval skin and maintain this functionality for weeks (Williams and Ribera, 2020). Zebrafish DRG neurons will eventually replace RBs as the primary somatosensory neurons innervating the skin; however, this transition takes place one to two months

Received Mar. 28, 2022; revised July 8, 2022; accepted July 19, 2022.

Author contributions: A.M.T., M.B.P., K.M.W., and A.V.N. designed research; A.M.T., M.B.P., and K.C.D. performed research; A.M.T., M.B.P., and A.V.N. analyzed data; A.M.T. wrote the first draft of the paper; A.M.T., M.B.P., K.M.W., and A.V.N. edited the paper; A.M.T. and A.V.N. wrote the paper.

This work was supported by the National Institute of Neurological Disorders and Stroke Grant R01 NS111419 and the Knight Cancer Institute (Knight Pilot Project; to A.V.N.). We thank Dr. Kelly Monk for generous access to her VAST sorting and confocal imaging system; Lindsey Royer for assistance in high-throughput imaging; Dr. Jeff Tyner for his gift of MKI drug screening reagents and Dr. Paul Brehm for providing the *SAIGFF213A* zebrafish line; and Dr. Adam Miller for critical manuscript review and feedback.

The authors declare no competing financial interests.

Correspondence should be addressed to Alex V. Nechiporuk at nechipor@ohsu.edu.

https://doi.org/10.1523/JNEUROSCI.0618-22.2022

postfertilization during bony scale formation (Rasmussen et al., 2018). Thus, zebrafish RBs offer unparalleled opportunities for *in vivo* examination of functional vertebrate somatosensory neurons with established axon terminals.

To disrupt signaling after cutaneous axon networks are established, we used multikinase inhibitor (MKI) small-molecule drugs. Each MKI inhibits multiple kinases at various affinities, creating a unique inhibition profile. The predominant target of MKIs are receptor tyrosine kinases (RTKs). One such RTK is c-Kit, a transmembrane type III RTK. It is activated on binding of its primary ligand, Stem Cell Factor/Kit-Ligand (SCF/KITLG). C-Kit receptor is expressed in a subset of rodent and primate DRG neurons that innervate embryonic and adult skin and KITLG is expressed in rodent adult skin (Hirata et al., 1995; Milenkovic et al., 2007; Usoskin et al., 2015; Kupari et al., 2021). Adult and embryonic mammalian studies have suggested possible roles for c-Kit signaling in DRG neurons (Milenkovic et al., 2007; Takagi et al., 2008; Sun et al., 2009), although its specific function in regulating cutaneous innervation of somatosensory neurons has not been established.

One downstream target of c-Kit is the Src family kinases (SFKs). SFKs are a group of non-RTKs that regulate signal transduction of many cell membrane receptors. SFKs bind activated c-Kit receptor (Voytyuk et al., 2003; Hong et al., 2004) to mediate its downstream signaling. Activated SFKs regulate axon outgrowth and guidance in vertebrates (Knöll and Drescher, 2004; Kao et al., 2009) and promote axon regeneration in multiple systems (Zhao et al., 2003; Nichols and Smith, 2020; Sakai et al., 2021). SFKs are particularly active in axon growth cone tips, where they regulate local tyrosine kinases that, in turn, impact filopodial/adhesion dynamics (Robles et al., 2005). However, the link between Kit signaling and SFK activity in peripheral axons has not been explored.

We find c-Kit receptor (*kitb* in zebrafish) is a major mediator of cutaneous axon maintenance and density. Treatment with MKIs targeting c-Kit leads to a loss of distal axon density in the skin and induces axon terminal retraction. Genetic loss of *kitb* leads to cutaneous axon density reduction, while hyperactivation of Kitb signaling induces highly-localized increases in axon density. Using DRG explant cultures, we find these effects of Kit inhibition are conserved in mammalian somatosensory neurons. Finally, we find that SFK activity downstream of Kitb is required for maintaining normal axonal density and activation of Kit signaling promotes axonal SFK activity. Thus, we establish c-Kit-SFK signaling as an important promoter of cutaneous axonal innervation and maintenance, as well as a potential mediator of the neurotoxicity of certain MKIs used in clinic to treat cancers.

Materials and Methods

Zebrafish husbandry

Adult zebrafish were maintained at 28.5°C as previously described (Westerfield, 2000). Embryos were derived from natural matings or *in vitro* fertilization, raised in embryo media, and developmentally staged (Kimmel et al., 1995). Strains used were *AB, *SAIGFF213A* [Muto et al., 2011; *UAS:GFP* ("*RB:GFP*")], and *kitb*^{sa15348} mutant (obtained from Zebrafish International Resource Center). The developmental stages used in this work are before sex specification and animals used in experiments are of indeterminate sex.

Genotyping protocols

kitb^{sa15348} mutants were genotyped by extracting genomic DNA from tail clips or whole larvae, then PCR amplifying with *Kitb F dCAP* and *Kitb R dCAP* primers that introduce a Hind III restriction site only in the amplicon of a mutant allele. PCR products were digested with Hind III-HF (New England Biolabs) for 4 h at 37°C, and run out on a 2% agarose TBE gel to resolve digested bands. Uncut amplicon is 399 bp, whereas HindIII digests mutant amplicon into 370- and 29-bp fragments.

Table 1. Oligonucleotides and primers

Oligo name	Sequence (5′ to 3′)
kitb 568/570Y-F IVA F	ACAGTTTTGATGGCAACAATTtTACCTtCATAGACCCAACGCAGC
kitb 568/570Y-F IVA R	ATTGTTGCCATCAAAACTGTCAATCACC
kitlgb F clone p221	GGGGACAAGTTTGTACAAAAAAGCAGGCTTCACCATGTTCCACATGAGGGAGG
kitlgb R clone p221	GGGGACCACTTTGTACAAGAAAGCTGGGTTGACCTCTGTGTCTGCACA
kitb dCAP F	CACCTCTTGCACAACAATGTCTAAC
kitb dCAP R HindIII	GACTCTGGTGCTAGCCGCACAACCAAGCT
kitb F clone p221	GGGGACAAGTTTGTACAAAAAAGCAGGCTTCACCATGGGACACTCGTGGTTTC
kitb R clone p221	GGGGACCACTTTGTACAAGAAAGCTGGGTTTATGCTCTGATGTTCCAGAAA
Kitb sgRNA	aattaatacgactcactataTGTGATCCTGATCCAAGACCgttttagagctagaaatagc
Ret sgRNA	aattaatacgactcactataGGTAAGACTGGGCTGGCCGAgttttagagctagaaatagc
Kitb CRISPR F	GTTTGTTTCCCTCAAAAACAGC
Kitb CRISPR R	GTGTTTGTGTCTAACCGCTTCA
Ret CRISPR F	ATGTAACGACATGTGCAAGACC
Ret CRISPR R	TAAAATGCTGAGCAGGACTCAC

CRISPR-Cas9-mediated genetic knock-down

sgRNAs for CRISPR-Cas9 knock-down of *kitb* and *ret* were designed (Table 1) and injections were performed as previously described (A.N. Shah et al., 2015) into *RB:GFP* embryos. CRISPR efficiency was evaluated by isolating genomic DNA from 3 days post fertilization (dpf) larvae, amplifying regions surrounding CRISPR target sites with respective CRISPR F and R primers (Table 1) and incubating amplicons with restriction enzymes that have cut sites adjacent to CRISPR targets (BslI for both *kitb* and *ret* sgRNAs). Digested amplicons were visualized by gel electrophoresis to ensure at least 75% of CRISPR-Cas9-injected larvae displayed total or significant loss in amplicon digestion, indicating efficient CRISPR-Cas9-mediated knock-down. At 3 and 5 dpf, *RB:GFP+* larvae that had obvious necrosis or body morphology defects were removed and tail tips of injected and uninjected larvae were rapidly imaged using the VAST-spinning disk microscope imaging system.

Drug treatment

Sorafenib, ponatinib, dasatinib, saracatinib, U73122, and LY294002 were obtained (Selleck Chemicals) and dissolved in DMSO to stock solutions of 10 mM and stored at −80°C. For larval treatment, drugs were diluted and mixed in embryo medium containing 1% DMSO and used to replace larval media. Unless otherwise noted, larvae were treated with drugs from 72–120 hpf, and larval media were replaced at 96 hpf with fresh drug/vehicle-containing media.

Plasmids, labeled constructs

To obtain template for cDNA cloning, total RNA was isolated from wild-type (WT) *AB embryos using Trizol reagent (ThermoFisher Scientific). First-strand cDNA synthesis was performed on 1 µg of total RNA using oligo dT primers and Superscript III reverse transcriptase (Invitrogen). Full-length zebrafish *kitb* and *kitlgb* were amplified with *kitb* and *kitlgb clone p221* F and R primers, respectively, and recombined into the Gateway middle entry vector pDONR221 using previously described methods (Kwan et al., 2007) to generate *pME:kitb* and *pME:kitlgb* plasmids. The double phosphosite mutant construct *pME:kitb*$^{Y568F/Y570F}$ was made by PCR using *pME:kitb* as a template and the *kitb 568/570Y-F IVA* F and R primers with the Phusion High-Fidelity PCR kit (ThermoFisher Scientific) followed by *in vitro* assembly in Top10 competent cells (ThermoFisher Scientific) as previously described (García-Nafría et al., 2016). Final plasmids were generated using the Gateway cloning method with pDestTol2pA2 destination vector and Tol2Kit plasmids (Kwan et al., 2007).

Zebrafish immunostaining

Larvae were anesthetized in 0.02% tricaine (MS-222; Sigma) in embryo medium, fixed in 4% formalin in 1× PBS for 1 h at room temperature (RT) and then 4°C overnight with one exception: larvae stained for α-pSFK Tyr418 were fixed in 1.5% formaldehyde in 0.1 M PIPES, 1.0 mM $MgSO_4$, and 2 mM EGTA for 1 h at RT, then 4°C overnight. Larvae were rinsed 3× with 1× PBS and permeabilized by washing in distilled water for 5 min, followed by 3× washes in 1× PBS + 0.1% Triton X-100 (PBTx). Larvae were incubated for 1 h at RT in blocking solution (PBTx + 5% goat serum, 1% bovine serum albumin, 1% DMSO), then at RT in primary antibody diluted in blocking solution for 2 h followed by 4°C overnight. Embryos were rinsed extensively in PBTx and incubated for 4 h at RT in Alexa488-conjugated, Alexa568-conjugated, or Alexa647-conjugated secondary antibodies diluted in blocking solution (1:1000, ThermoFisher Scientific). After rinsing in PBTx, larvae were transferred to 70% glycerol in PBS and mounted on slides with 0.13–0.17 mm borosilicate coverslips secured with vacuum grease. Primary antibodies used were α-pSFK Tyr418 (1:500, Invitrogen, 44660G, RRID:AB_1500523), α-mCherry (1:1000, ThermoFisher Scientific, M11217, RRID:AB_2536611), α-GFP (1:1500, Aves Labs, RRID:AB_10000240), α-Cleaved Caspase-3 (1:1000, Cell Signaling, 9664P, RRID:AB_2070042), and α-acetylated Tubulin (1:1000, Sigma-Aldrich, T6793, RRID:AB_477585).

Confocal fluorescence imaging of zebrafish larvae

For live imaging, larvae were mounted in 1.5% low melting point agarose on a glass coverslip, submerged in embryo media containing 0.02% tricaine (MS-222; Sigma) and imaged using a 40×/NA = 0.8 water immersion objective on an upright Fluoview1000 confocal microscope (Olympus) with 488- and 568-nm excitation channels. To assess RB neuron apoptosis over time, RB neuron cell bodies in the dorsal spinal cord of *RB:GFP* embryos were imaged at 10 min/frame for 15 h in an ~400-μm-wide viewing window. For imaging sparsely labeled RB neurons over time and the axonal effects of Kitlgb misexpression, *RB:GFP* embryos were injected at one-cell stage with *UAS:mCherry* or *Krt4:kitlgb-p2a-mCherryCAAX* plasmids, respectively. Larvae injected with *UAS:mCherry* that contained caudal tail axons expressing mCherry at 3 or 4 dpf were mounted, submerged in embryo media containing vehicle or drug, and imaged 5 min/frame over 10 h. *RB:GFP* larvae injected with *Krt4:kitlgb-p2a-mCherryCAAX* were screened for presence of mCherry+ skin cells and the mCherry+ regions and mCherry– adjacent regions were imaged. Immunostained larvae were imaged on the Olympus Fluoview1000 with 488-, 568-, and 647-nm excitation channels. For cleaved Caspase-3 immunostained larvae, a 20×/NA = 0.75 air objective was employed and for pSFK immunostained larvae, a 60×/NA = 1.42 oil immersion objective was used.

High-throughput fluorescence larval imaging

For live high-throughput imaging caudal tails of WT, *kitb* mutant, or drug-treated *RB:GFP* larvae, we used the Large Particle (LP) Sampler and VAST BioImager (Union Biometrica) to automate the delivery of zebrafish from 96 multi-well plates to the BioImager microscope platform as previously described (Early et al., 2018). Z-stacks of 218 frames with a step size of 1.84 μm were acquired using Zen Blue 2.0 software (Carl Zeiss).

Axon density quantification

Based on the large volume of data produced by high throughput imaging, we designed a streamlined system for measuring axonal density using open-source software. We imported confocal images of *RB:GFP* caudal tails into FIJI (Schindelin et al., 2012), converted images to 8-bit, and generated maximum intensity Z-projections. We then thresholded the projections, formed a rectangular 50 × 100 μm region of interest (ROI) at the distal tail tip, and measured the percentage of this ROI occupied by GFP+ axons.

To quantify changes in axonal density in cutaneous tissue misexpressing Kitlgb, we generated max-intensity Z-projections of imaged regions of *Krt4:kitlgb-p2a-mCherryCAAX*-injected larvae and made ROIs using the boundaries of mCherry+ and adjacent mCherry– regions of skin cells in FIJI. Percent area measurements of *RB:GFP*-labeled axons in adjacent mCherry+/mCherry– regions were taken as described and compared within individual larvae.

Immunofluorescence intensity quantification

For consistency of labeling, compared larvae were processed in the same batch. To quantify axonal pSFK staining, *RB:GFP* larvae were immunostained with α-pSFK, α-GFP, and α-acetylated Tubulin (AcTu). 3D reconstructions of larvae axonal volumes were generated in Imaris (Bitplane) using GFP immunofluorescence channel signal. For quantifying pSFK changes in the caudal tail, we measured mean fluorescence intensity (MFI) of pSFK and AcTu within axons in a 50 × 100 μm ROI at the distal tip of the tail. To account for sample-to-sample variation in permeability and staining intensity, we normalized pSFK MFI to the ratio of the AcTu MFI of an individual larva divided by the average of the AcTu MFI within an experimental group. To prepare 2D images of pSFK immunostaining solely in axons, we generated a masked channel containing only pSFK signal within the 3D-reconstructed axons, and made max intensity Z-projections for each channel in Imaris.

To quantify axonal fluorescence intensity of pSFK staining in cutaneous regions misexpressing Kitlgb-p2a-mCherryCAAX, we identified immunostained larvae containing regions of one to two isolated mCherry+ skin cells. These regions (one to two per larva) were imaged and axonal volume was reconstructed in Imaris as described. Axonal pSFK MFI was measured within mCherry+ regions and within two adjacent, mCherry– regions of comparable size 30 μm away (approximately one skin cell length). Within a single larva, MFI of mCherry+ and mCherry– regions were separately averaged and then compared.

Axon terminal dynamics analysis

Distance of all distal axon terminals from tail edge that were within 50 μm of the distal caudal tail edge at $t = 0$ per labeled RB neuron were measured at $t = 0$ and $t = 10$ h and averaged for each neuron ($n = 5$ total neurons in ≥3 larvae per condition). For kymograph generation, analysis, and visualization, we used the MetaMorph software package (Molecular Devices) as previously described (Drerup and Nechiporuk, 2016; Tuttle et al., 2019) with one difference: instead of analyzing movement of individual, labeled particles, we examined single axon terminals labeled by *UAS:mCherry* in *RB:GFP* larvae to visualize net movement relative to the nearest tail edge over time.

Scoring apoptotic RB neurons

RB:GFP+ WT or *kitb* mutant larvae were fixed at 30 or 48 hpf, immunostained for cleaved-Caspase-3, and imaged from otic vesicle to the end of the spinal cord. We counted *RB:GFP*+ and cleaved-Caspase-3+ neurons in the dorsal-most portion of the spinal cord, where only RBs should be present. For time-lapse imaging of RB neuron cell bodies, the posterior-most edge of the 400-μm viewing window was placed in line with the end of the yolk extension. RB neurons were identified by spinal cord location, morphology, and axonal projections and apoptotic/dying neurons were counted. Counts per viewing window were normalized to 50-μm length.

Plate and coverslip preparation for DRG culture

DRG explants were grown on glass coverslips in 12-well tissue culture plates. Coverslips were incubated overnight at 4°C in 100 μg/ml poly-D lysine in cell culture grade water, washed twice, incubated at 37°C with 10 μg/ml mouse Laminin (ThermoFisher, 23017015) for 5 h, washed twice, and allowed to dry for 5–10 min before plating.

In vitro *DRG explant culture*

DRG explant cultures were performed on Embryonic day 15.5 (E15.5) CD1 mouse embryos. DRG from a single embryo were isolated through fine dissection as previously described (Hall, 2006). After washing DRGs were suspended in DRG plating media (Neurobasal media, ThermoFisher, 21103049), 35 mM glucose, 2% B27 supplement (ThermoFisher, 17504044), 1% GlutaMAX supplement (ThermoFisher, 35050061), 1% penicillin/streptomycin, 50 ng/ml SCF (Proteintech,

HZ-1024) run through a 0.22-µm syringe filter. DRGs were resuspended in DRG plating media and were spot plated onto coated glass coverslips (~20-µl spots containing one to two DRG explants/coverslip). Plates were incubated for 1 h at 37°C with 5% CO_2 before gently flooding the wells of the plate with DRG plating media.

After 24 h of growth, a media change was performed with half the plated volume of media and treatment drugs were added at appropriate concentrations in DMSO. Cultures were allowed to grow for another 24 h before fixation for 30 min at RT by adding one plating volume of 4% paraformaldehyde-Krebs solution-sucrose fixative (4% w/v paraformaldehyde, 145 mM NaCl, 5 mM KCl, 1.2 mM $CaCl_2$-$2H_2O$, 1.3 mM $MgCl_2$-H_2O, 1.2 mM NaH_2PO_4-H_2O, 10 mM glucose, 20 mM HEPES, and 0.4 M sucrose, in H_2O) for a final paraformaldehyde concentration of 2%.

Explant immunolabeling, imaging, and quantification

Fixed and washed explant containing coverslips were incubated for 30 min in blocking buffer (0.2% Triton X-100, 5% normal donkey serum, 0.002% NaN_3, 5% DMSO, in phosphate-buffered saline) at RT and incubated in blocking buffer with primary antibody (rabbit α-β-III Tubulin, Millipore Sigma T2200-200UL, 1:1000, RRID: AB_262133) overnight at 4°C. Nuclei were labeled with Hoechst 33 342 (1:5000 in PBS, Life Technologies H3570) included in the first wash after primary incubation. Fluorescent secondary antibodies (donkey α-rabbit 488 or donkey α-rabbit 546, ThermoFisher A-21206 or A-10040) were applied for 4 h at RT. Coverslips were mounted to glass slides for imaging using Fluoromount-G (Fisher, OB100-01). Explants were imaged on a Zeiss AxioImagerM.2 upright microscope using a 5× objective. Quantification was performed in FIJI (Schindelin et al., 2012). The cell body core outline in the explant center was traced manually and a ROI was generated by expanding this traced shape 50 µm and using the FIJI "Make Band" function to generate a 50-µm-wide band. The image was then manually thresholded and the coverage density of the 50-µm-wide band was measured.

Experimental design and statistical analysis

The sex of the animals was unknown as sex specification has not occurred at this stage of larval development. Analysis was performed with Prism software (GraphPad). Specific statistical tests and *post hoc* tests for each data set are indicated in text and figure legends. For experiments involving two independent variables, two-way ANOVA tests were performed to test whether main effects and interactions were statistically significant. If interaction was statistically significant, ANOVA was repeated with simple effects, and significance of main effects was re-evaluated and the indicated *post hoc* tests were performed. Results were considered statistically significant when $p < 0.05$. Data in text or plotted with error bars on graphs were expressed as mean ± SEM.

Study approval

All animal works were approved by and conducted according to guidelines of the Oregon Health and Science University Institutional Animal Care and Use Committee, protocol# IP00000495.

Results

MKI treatment induces loss of cutaneous sensory axon innervation

In order to visualize cutaneous RB axons *in vivo*, we used zebrafish larvae carrying two transgenes: *SAIGFF213A* (a GAL4 driver that labels distinct types of neurons, including the RBs; Muto et al., 2011) and a UAS:GFP reporter (this double transgenic line hereafter referred to as *RB:GFP*). By 48 hpf, GFP+ RB axons have reached the tail tip, arborized, and extended along the perimeter of the caudal tail edge (Fig. 1*A*,*B*). Although early reports of RBs suggested they may die off rapidly by 5 dpf (Williams et al., 2000), more detailed analysis from several groups suggests this is not the case. Recent studies have established that this experimental window, 3–5 dpf, consists of stable, established RB axon networks in the tail with no significant loss of RB axons or RB cell death specifically in the RBs that innervate the tail tissue (Rasmussen et al., 2018; Williams and Ribera, 2020). Because of the stable nature of these established tail axons during this time period, they have become a powerful *in vivo* model for examining neuropathic effects of chemotherapy drugs (Lisse et al., 2016; Cirrincione et al., 2020) or regeneration of cutaneous axons following injury (Rieger and Sagasti, 2011). This is consistent with our time-lapse observations (see Figs. 2 & 3 below), where we found no notable loss of major axon arbors in the tail during this time in control or drug-treated larvae that would be the result of cell death of RBs that innervate this tissue.

To identify signaling pathways important in somatosensory axon maintenance, we treated larval zebrafish with several MKI drugs that have been associated with sensory neurologic side effects in human patients. These types of drug-induced peripheral neuropathic side effects are often thought to be, at least in part, because of axonal degeneration/retraction or a failure of axonal maintenance (Fukuda et al., 2017). Larvae were treated

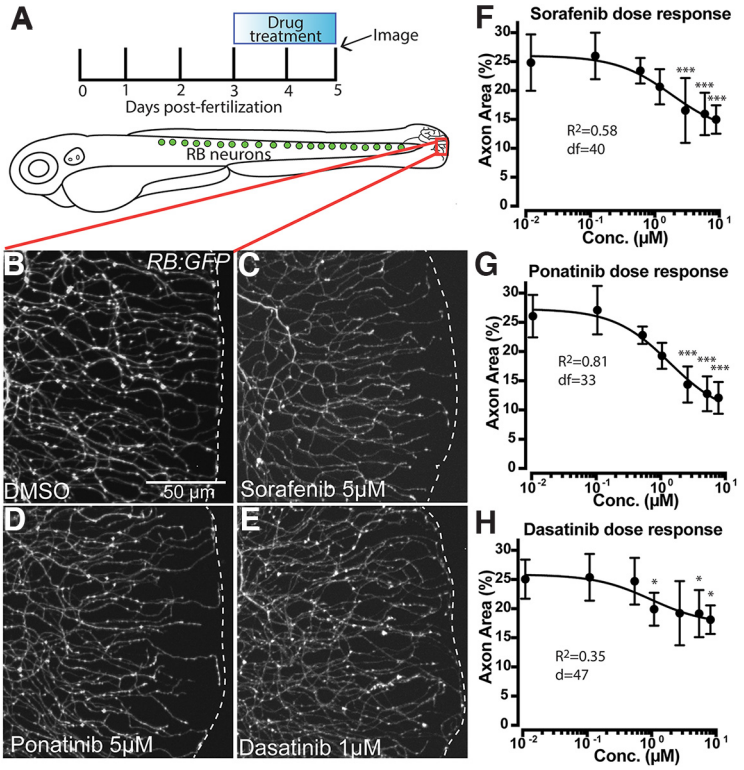

Figure 1. Treatment with MKIs induces loss of cutaneous axon density in zebrafish caudal tail. ***A***, Diagram of RB neurons, drug treatment and imaging paradigm, and imaging location (red box). ***B–E***, Live images of somatosensory axons at the caudal tail tip labeled by *RB:GFP* after 48 h of treatment. Several MKIs produced significant loss of cutaneous axon density (white dashes indicate tail edge). ***F–H***, Dose-dependent loss of distal axon density induced by (***F***) sorafenib, (***G***) ponatinib, and (***H***) dasatinib treatment, analyzed by one way ANOVA with *post hoc* Dunnett's test versus the lowest dose. Error bars represent SEM; $*p < 0.05$, $***p < 0.001$.

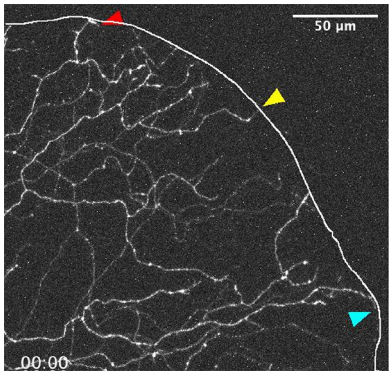

Movie 1. Time-lapse imaging of RB axons during control DMSO treatment. White line indicates tail edge. [View online]

for 48 h, then GFP-labeled axons of the distal caudal tail tip were imaged (Fig. 1*A*,*B*). We chose 72 hpf as the beginning of the drug treatment window, after cutaneous distal axon outgrowth and arborization has stabilized. To quantify axonal density within the thin skin of the distal tail, we used ImageJ to create a maximum intensity Z-stack projection and measured the proportional area of a 50×100 µm region of interest at the tip of the tail occupied by GFP-labeled axons. We identified three MKIs that induced significant, dose-dependent loss of distal axonal density in the tail compared with vehicle controls: sorafenib, ponatinib, and dasatinib (Fig. 1*C*–*H*). These changes in axon density suggest these MKIs disrupt normal axonal maintenance.

Axon terminal retraction underlies MKI-induced axon loss

To determine the cellular bases for the loss of cutaneous axon density, we performed time-lapse imaging of sparsely-labeled RB axons in the caudal tail. Injection of a UAS:mCherry plasmid at one-cell stage in *RB:GFP* embryos mosaically labeled RB neurons and allowed imaging of axon terminals in the caudal tail from individual neurons during drug treatment. Control RB axon terminals are dynamic and often extend, retract, and explore over time (Movie 1; Fig. 2*A*). Compared with vehicle treatment, application of sorafenib and ponatinib induced notable retraction of individual axon terminals over a period of 10 h, although terminal behavior was still dynamic (Movies 2, 3; Fig. 2*B*,*C*). To analyze the movement of these time-lapse imaged individual axon terminals, we performed kymograph analysis on distal terminals. Kymographs show consistent, active proximal movement of terminals away from the tail edge during drug treatment (Fig. 2*D*–*F*). Quantification of the net movement of distal axon terminals over time found that control terminals exhibited minor net terminal extension over 10 h, while sorafenib and ponatinib treatment both induced significant net retraction from the initial position (Fig. 2*G*; DMSO = 1.5 ± 1.1 µm net distal movement, sorafenib = −6.6 ± 0.7, ponatinib = −4.4 ± 1.2). The net active movement of drug-treated axon terminals proximally (away from their initial position), as opposed to remaining stationary, suggests significant retraction and not a failure of outgrowth. To address the possibility that MKI treatment affected normal increases in distal axon arborization or growth between 3 and 5 dpf, we performed repeated measures of distal axon density of individual control larvae during the drug treatment window and found no significant changes in distal tail axon density from 3 to 5 dpf (Fig. 2*H*). Taken together, these data indicate that the loss of axon density following MKI treatment is because of axon terminal retraction.

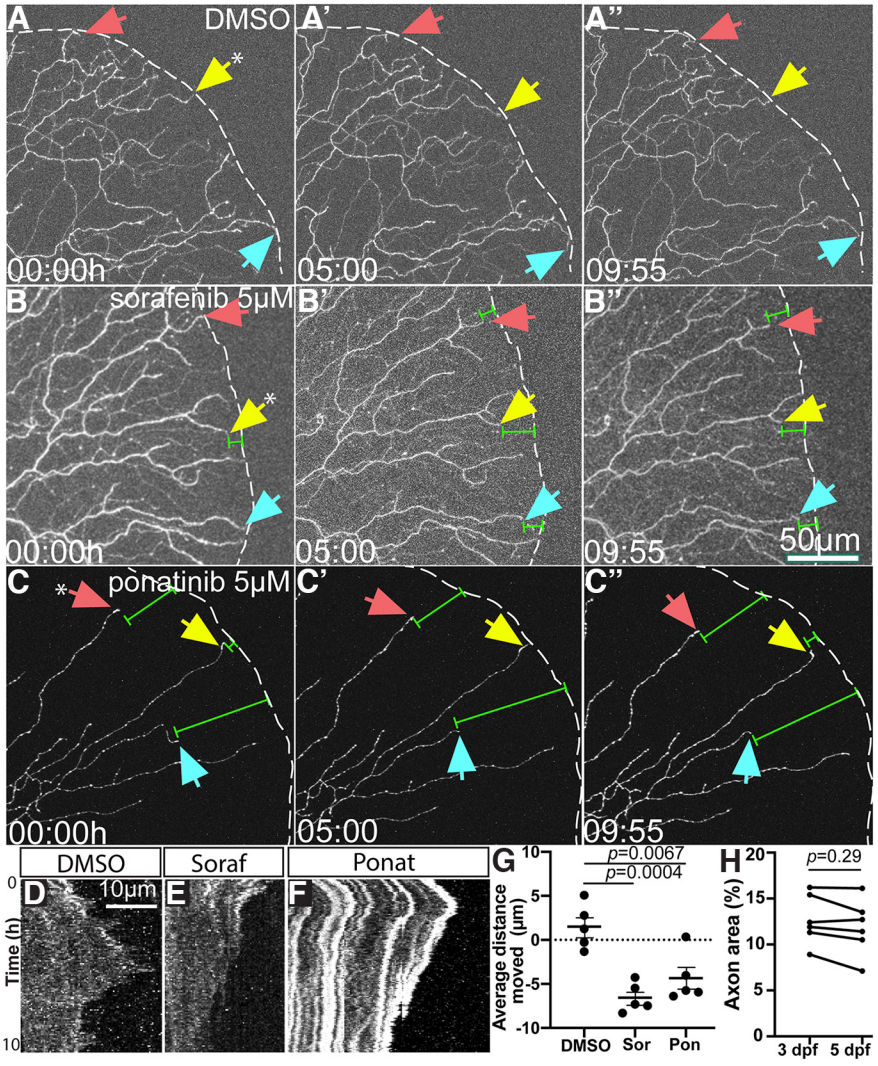

Figure 2. Time lapse imaging reveals axon terminal retraction following sorafenib and ponatinib treatment. ***A–C***, Stills from Movies 1, 2, 3, respectively, of distal axons of sparsely labeled RB neurons. Over 10 h, sorafenib and ponatinib treatment induced retraction of distal axon tips (white dashes = tail edge, arrows indicate specific axon terminals followed over time, green measurement bars indicate distance from edge). ***D–F***, Kymographs of individual axon terminals (indicated by asterisk in panels ***A–C*** from respective movies. DMSO terminals (***D***) show dynamic extension and retraction, but sorafenib (***E***) or ponatinib (***F***) treatment induce notable net retraction of axon terminals. ***G***, Quantification of axon retraction in 10-h time lapse movies. Compared with DMSO-treated larvae that had a net increase in axon outgrowth, sorafenib and ponatinib treatment induced a significant net retraction of distal RB axon terminals in labeled neurons by one-way ANOVA with *post hoc* Dunnett's test. Error bars represent SEM. ***H***, Repeated measures of axonal density of WT control larval tails analyzed by paired *t* test from 3 to 5 dpf had no difference: 3 dpf = 12.3 ± 1.1% axon area, 5 dpf = 11.9 ± 1.2.

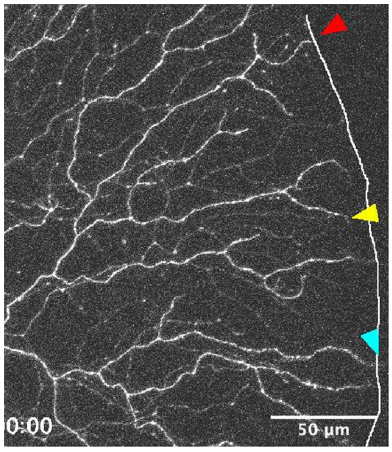

Movie 2. Time-lapse imaging of RB axons during sorafenib treatment. White line indicates tail edge. [View online]

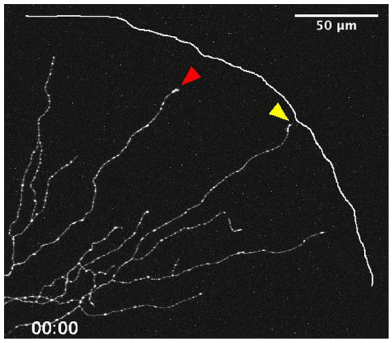

Movie 3. Time-lapse imaging of RB axons during ponatinib treatment. White line indicates tail edge. [View online]

Loss of Kitb receptor phenocopies drug treatment

Although we observed similar phenotypes from treatment with sorafenib, ponatinib, and dasatinib, the molecular targets underlying this effect were unknown. MKIs can target a range of kinases, but RTKs are often the primary targets of many MKIs. We searched the literature for the common RTK targets of sorafenib, ponatinib, and dasatinib that are reported to be highly inhibited ($IC_{50} \leq 100$ nM *in vitro*; Adnane et al., 2006; N.P. Shah et al., 2006; Plaza-Menacho et al., 2007; O'Hare et al., 2009; Mologni et al., 2013). Among these RTKs, c-Kit and Ret are specifically expressed in zebrafish RBs (Marcos-Gutiérrez et al., 1997; Mellgren and Johnson, 2005). c-Kit is a major inhibitory target of all three MKIs. Furthermore, c-KIT and RET are reported to be expressed in mammalian unmyelinated nociceptive DRG neurons with roles in neurodevelopment, regeneration, and/or pain sensation (Sun et al., 2009; Golden et al., 2010; Usoskin et al., 2015; Barkai et al., 2019; Tavares-Ferreira et al., 2021). We chose these receptors as candidates for RTKs that may underlie the axonal effects of these MKIs and examined them for roles in zebrafish RB neurons.

Zebrafish have two paralogues of c-Kit, *kita* and *kitb*, but only *kitb* is specifically expressed in the RB neurons (Hultman et al., 2007). In *RB:GFP* larvae, transient CRISPR-Cas9-mediated knock-down of Kitb induced a significant loss of caudal tail axon density at 3 and 5 dpf (Fig. 3*A*). Notably, knock-down of the other candidate expressed in RBs, Ret, had no effect on somatosensory axons in the caudal tail (Fig. 3*A*). To confirm the transient Kitb knock-down phenotype, we obtained a zebrafish mutant line ($kitb^{sa15348}$), containing a premature stop in *kitb* (Y197X). *RB:GFP* transgenic larvae homozygous for the *kitb* mutant allele had significantly reduced tail cutaneous axon density at 3 dpf compared with WT siblings (Fig. 3*B–D*, WT = 13.4 ± 0.6%axonal area vs *kitb* mutant = 7.9 ± 0.7). Injection of 25 pg of *kitb-p2a-mCherry* mRNA into *kitb* mutant or sibling embryos at the one cell stage significantly suppressed the loss of tail innervation in *kitb* mutants by 3 dpf (Fig. 3*D*), demonstrating that loss of *kitb* is indeed responsible for this phenotype. To address whether this loss of axon density was because of premature RB death, we performed live imaging analysis and Caspase-3 immunolabeling in *kitb* mutants and WT siblings. We observed no significant changes in RB apoptosis during time-lapse imaging (30–45 hpf; Fig. 3*E*, sibling = 0.4 ± 0.1 apoptotic neurons/50 µm, *kitb* = 0.3 ± 0.1). Furthermore, we found a significant decrease in the number of neurons positive for cleaved Caspase-3 staining in *kitb* mutants at 30 hpf, although there was no significant change in the number of Casp3+ RB neurons at 48 hpf (Fig. 3*F–J*, 30 hpf: siblings = 1.1 ± 0.3 neurons, *kitb* = 0 ± 0; 48 hpf: sibling = 0.3 ± 0.3, *kitb* = 0.8 ± 0.4). These data indicate Kitb is a regulator of cutaneous somatosensory axon innervation in zebrafish larvae and that the reduction in cutaneous axon density in *kitb* mutants was not because of premature RB neuron death.

Kitb is a major neural target of MKIs

In order to test whether Kitb is a major target that mediates the effects of these MKIs on sensory axons, we treated *RB:GFP kitb* mutant or sibling larvae with either vehicle, sorafenib, ponatinib, or dasatinib. If Kitb primarily mediates the observed sorafenib-induced, ponatinib-induced, or dasatinib-induced axonal loss, we expected genetic removal of Kitb would preclude additional neuropathic effects from drug treatment. In accordance with this, we observed no significant exacerbation of the axon density loss at 5 dpf in *kitb* mutants treated with any of the individual MKIs compared with vehicle-treated *kitb* mutants (Fig. 3*K–M*). There was also no significant difference between vehicle-treated *kitb* mutants and sorafenib/ponatinib-treated WT larvae, although dasatinib-treated WT larvae had less axon density reduction than vehicle-treated or dasatinib-treated *kitb* mutants. Altogether, these data suggest that Kitb is a specific, major target of sorafenib, ponatinib, and dasatinib that mediates their effect on density of sensory axon terminal networks.

Kitb has an early role in regulating cutaneous axon density

We next investigated whether Kitb had a role in regulating cutaneous axon behavior before 3 dpf. Examining distal RB axons at 24 hpf, we found that *kitb* axons initially extend and branch in the distal tail similar to WT (Fig. 4*A*,*B*). There was no significant difference in the number of axonal terminals nor the number of primary axon branches in WT compared with *kitb* mutants (Fig. 4*G*, *H*; axon terminals: WT = 23.9 ± 2.9 terminals vs *kitb* = 20.8 ± 2.2; primary axon branches: WT = 5.4 ± 0.4 branches vs *kitb* = 4.8 ± 0.3). *kitb* axons also extended fully to the distal tail edge and elongated around the perimeter similar to WT by 36 and 48 hpf (Fig. 4*C–F*); however, their distal axonal density was significantly reduced compared with WT controls (Fig. 4*I*; 36 hpf: WT = 10.5 ± 0.7% axon area vs *kitb* = 8.5 ± 0.6; 48 hpf: WT = 13.3 ± 0.9 vs *kitb* = 8.7 ± 0.5). These data suggest that *kitb* is not required for initial cutaneous axon extension and growth but does have a role in regulating axonal density early in development.

Kit ligand b promotes local cutaneous axon innervation

c-Kit is expressed in a subset of mammalian DRG neurons, largely peptidergic unmyelinated C-fibers (Usoskin et al., 2015)

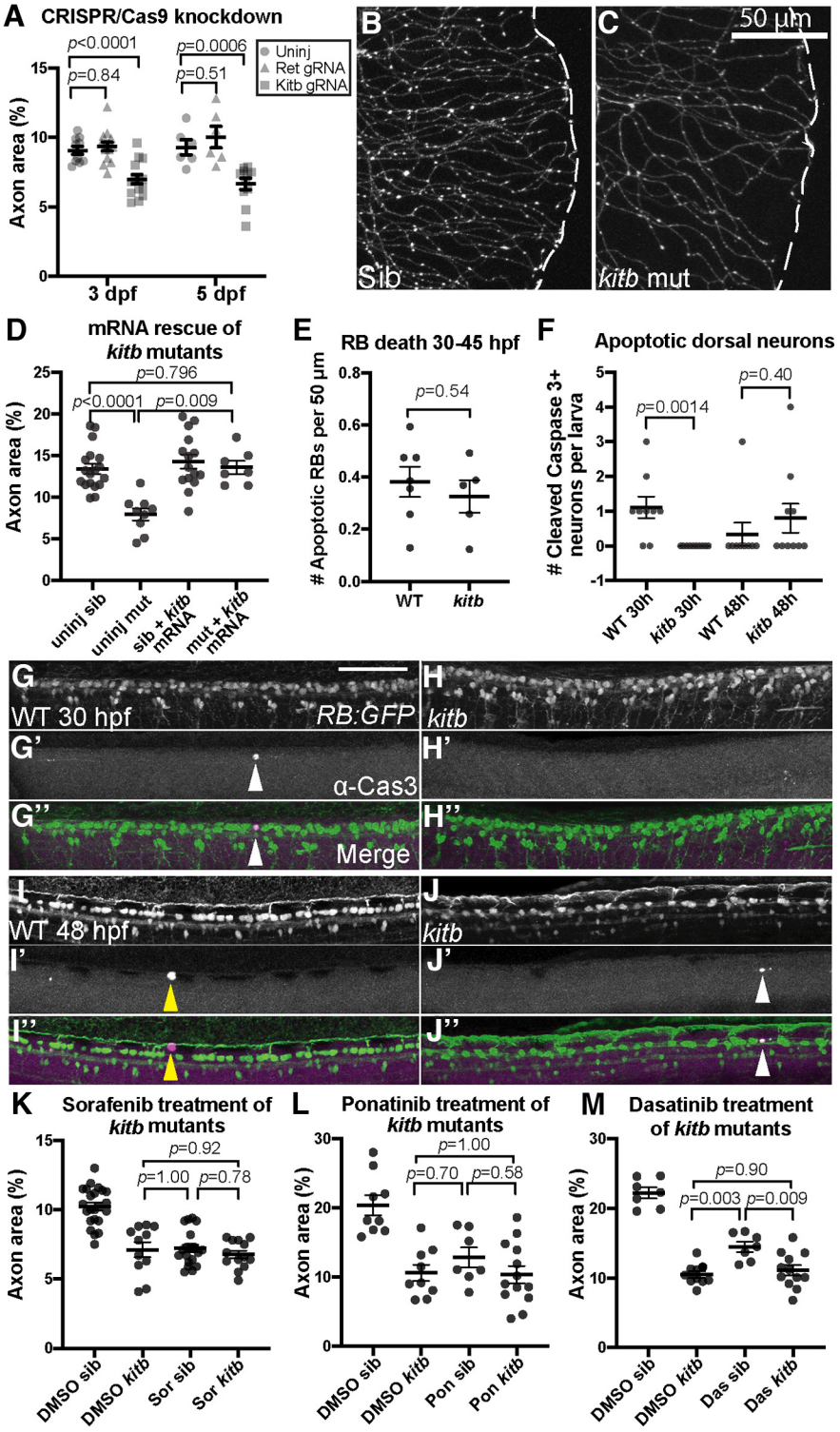

Figure 3. *kitb* is a major target mediating cutaneous axonal effects of several MKIs. ***A***, Quantification of distal cutaneous axon density in caudal tail after CRISPR-Cas9-mediated knock-down of either *ret* or *kitb*; 3 dpf: uninjected = 9.1 ± 0.3% area, *ret* gRNA= 9.3 ± 0.3, *kitb* gRNA = 7.0 ± 0.3; 5 dpf: uninjected = 9.3 ± 0.5%, *ret* gRNA= 10.3 ± 0.9, *kitb* gRNA = 6.7 ± 0.4. ***B***, ***C***, Live imaging at 5 dpf of *kitb* homozygous mutants or siblings (sib) in the *RB:GFP* transgenic background (white dashes = tail edge). ***D***, Expression of *kitb* mRNA suppresses *kitb* mutant axon density defect. Uninjected sib = 13.4 ± 0.6% area, uninjected mutant = 7.9 ± 0.7, *kitb* mRNA sib = 14.9 ± 0.9, *kitb* mRNA mutant = 13.6 ± 0.8. ***E***, Quantification of time-lapse observation of RB cell death during embryonic development, analyzed with unpaired *t* test. Error bars represent SEM. There was no significant difference in the number of RB neurons undergoing apoptosis between *kitb* mutants and siblings. ***F***, Quantification of Cleaved-Caspase-3+ dorsal neurons in immunostained *RB:GFP* WT and *kitb* mutant larvae, analyzed by unpaired Student's *t* test at each time point. There was no significant difference in GFP+/cleaved-Caspase-3+ dorsal neuron number in *kitb* mutants at 48 hpf compared with siblings but at 30 hpf, there were significantly fewer of these cells detected

and a subpopulation of myelinated mechanoreceptors (Milenkovic et al., 2007). While data suggest c-Kit has roles in somatosensory neuron survival/differentiation or in nociceptive sensitization, its specific role in somatosensory cell biology and function is still largely unsettled (Lourenssen et al., 2000; Takagi et al., 2008; Sun et al., 2009). The c-Kit ligand, SCF/KITLG, is expressed in the skin of mammalian adults, suggesting a potential role in maintenance or promotion of cutaneous sensory axon density. Similar to the c-Kit receptor, zebrafish have two paralogues of SCF/KITLG: Kit ligand a and b (Kitlga/b), each of which primarily activates and binds its respective receptor because of biochemical selectivity (Yao and Ge, 2013). At larval stages in the trunk, *kitlga* is expressed in the developing sense organs and pigment precursors, whereas *kitlgb* is expressed in the skin, similar to mammalian SCF/KITLG expression (Hultman et al., 2007). Recent single-cell RNA-seq (Metikala et al., 2021) and bulk RNA-seq of different skin layers (Cokus et al., 2019) of embryonic and larval zebrafish indicate that both layers of the zebrafish skin, the basal cells and periderm, express Kitlgb at 30, 52, and 72 hpf. In particular, expression levels of Kitlgb at 52 and 72 hpf are virtually the same in both skin cell populations (Cokus et al., 2019). To explore the effect of skin-produced Kitlgb on cutaneous axon density, we cloned *kitlgb* and generated a plasmid expressing Kitlgb with a cleavable membrane-localized mCherry under the

←

in *kitb* mutants. ***G–J***, Images of cleaved-Caspase-3 immunostaining in dorsal trunks of fixed *RB:GFP* larvae at 30 hpf (***G***, ***H***) and 48 hpf (***I***, ***J***). Scale bar: 100 µm; white arrowheads=cleaved-Caspase-3+ dorsal neurons, yellow arrow heads = cleaved-Caspase-3+ non-neurons. ***K–M***, Quantification of *kitb* mutants treated with either sorafenib (***K***), ponatinib (***L***), or dasatinib (***M***) using the same treatment paradigm from Figure 1*A*. While treatment with either drug or genetic loss of *kitb* induced loss of cutaneous axon density, treatment of *kitb* mutants with drug did not exacerbate this phenotype, indicating Kitb is a major target underlying their peripheral neurotoxicity in this case. Two-way ANOVA with *post hoc* Tukey's HSD test for datasets. ***K***, DMSO sib = 10.2 ± 0.3% area versus DMSO *kitb* = 7.1 ± 0.5, $p < 0.0001$; versus sorafenib sib = 7.2 ± 0.3, $p < 0.0001$; versus sorafenib *kitb* = 6.8 ± 0.3, $p < 0.0001$. ***L***, DMSO sib = 20.4 ± 1.5% area versus DMSO *kitb* = 10.6 ± 1.2, $p < 0.0001$; versus ponatinib sib = 12.9 ± 1.4, $p = 0.0051$; versus ponatinib *kitb* = 10.4 ± 1.2, $p < 0.0001$. ***M***, DMSO WT = 22.2 ± 0.8% versus DMSO *kitb* = 10.5 ± 0.5, $p < 0.0001$; versus dasatinib WT = 14.5 ± 0.7, $p < 0.0001$; versus dasatinib *kitb* = 11.1 ± 0.7, $p < 0.0001$. Error bars represent SEM.

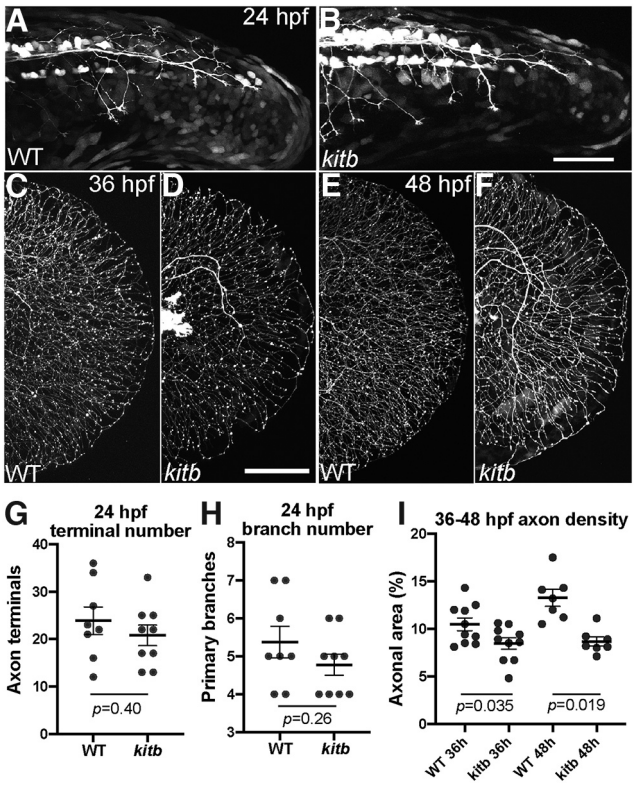

Figure 4. *Kitb* mutants exhibit reduced axon density following normal initial extension. ***A–F***, Live lateral images of *RB:GFP* tail regions from 24 to 48 hpf. Scale bar: 50 μm. ***A***, ***B***, WT and *kitb* mutants exhibit similar RB axon extension and early branching in distal tail at 24 hpf. ***C–F***, WT and *kitb* mutant RB axons fully extend to the distal caudal tail and grow along the perimeter by 36 and 48 hpf; however, *kitb* mutants have reduced distal axonal density by 36 hpf and beyond. Scale bar: 50 μm. ***G***, ***H***, Quantification of RB axon terminal number and primary branch number at 24 hpf in the distal 200 μm of the tail. There was no significant difference between WT and *kitb* mutants in distal terminal number (***G***) or branch number (***H***), indicating axon growth and extension were normal. ***I***, Quantification of distal axonal density at 36 and 48 hpf: *kitb* mutants had significantly reduced axonal density of the distal caudal tail compared with WT. Error bars represent SEM.

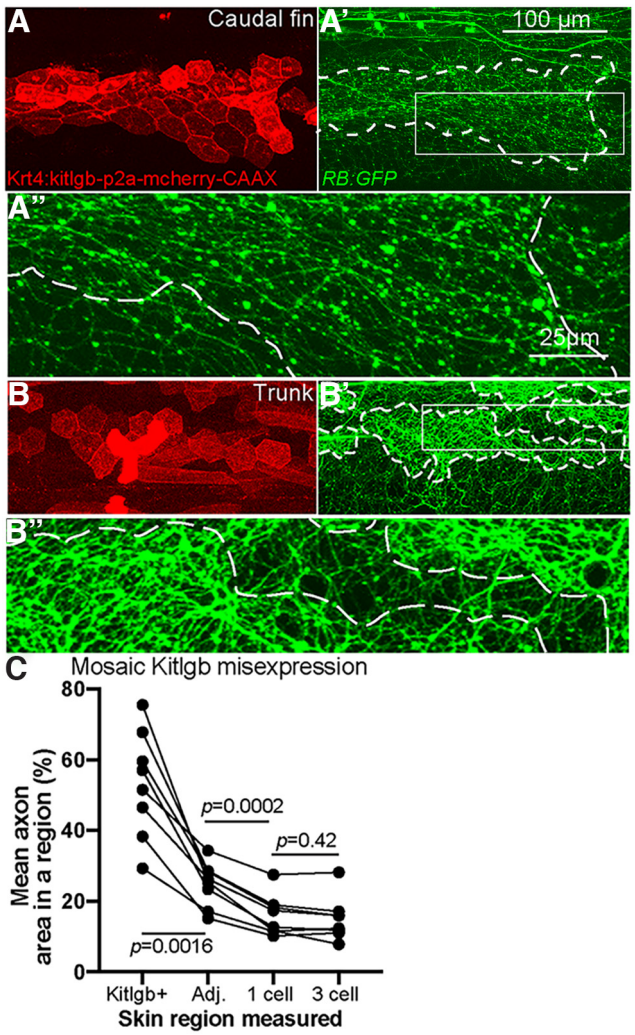

Figure 5. Overexpression of Kit ligand b increases local axon density. ***A***, ***B***, Live imaging at 4 dpf of larvae injected with plasmid expressing *kitlgb* under a skin promoter. ***A′***, ***B′***, RB axons, labeled by *RB:GFP*, are significantly denser in regions of skin cells overexpressing *kitlgb* (white dashes indicate Kitlgb/mCherry+ regions). ***A″***, ***B″***, 4× magnified insets of ***A′***, ***B′***. ***C***, Quantification of axon density within individual larvae mosaically expressing Kitlgb (repeated measures ANOVA). Comparison of average axonal area within Kitlgb/mCherry+ regions (Kitlgb+), directly adjacent regions (Adj.), 1 cell length distance or 3 skin cell length distance from mCherry+ skin cells. Kitlgb+ = 53.2 ± 5.4% axonal area, Kitlgb–adjacent region =24.8 ± 2.2, 1 cell length distance = 16.0 ± 2.0, 3 cell length distance =15 ± 2.2. Kitlgb-misexpressing regions had significantly higher axonal density than any other region, while directly adjacent regions also had higher density than regions further away.

keratin 4 (*krt4*) skin promoter (krt4:kitlgb-p2a-mCherryCAAX) that expresses strongly in both larval zebrafish skin layers. Microinjection of this plasmid into RB:GFP embryos at one-cell stage produced larvae with mosaic patches of mCherry+ skin cells (Fig. 5*A*,*B*) in both skin layers. Misexpression of Kitlgb in these regions induced dramatic, significant local increases in RB axon density compared with adjacent, mCherry– regions (Fig. 5). These increases in axonal density were highly localized when compared with axon density one to three skin cell diameters away (one skin cell diameter is ~30 μm; Fig. 5*C*). Interestingly, axon density was still higher in regions immediately adjacent to the overexpression domain compared with one and three cell diameters away (Fig. 5*C*), indicating that Kitlgb has a localized effect. Together with receptor loss-of-function data, this suggests that cutaneous Kitlgb promotes increased somatosensory axon density in a highly localized manner; however, this does not affect axonal density in more distal skin regions.

MKIs reduce SFK activity in distal RB axons

There are several major downstream signaling pathways of activated Kit receptor, including phosphoinositide-3 kinase (PI3K), phospholipase C (PLC) enzymes, and SFKs (Hong et al., 2004). Forty-eight-hour treatment with inhibitors of PI3K or PLCγ commonly used in zebrafish and other systems, LY294002 and U73122, respectively, had no significant effect on distal axonal cutaneous density (Fig. 6*A*,*B*). In contrast, treatment with saracatinib, a potent SFK inhibitor (Green et al., 2009), led to reductions in distal axon density similar to MKI treatment (Fig. 6*C*), suggesting SFK activity is a regulator of axonal density. One SFK in particular, Src, is well-established as a regulator of axon pathfinding and outgrowth (Robles et al., 2005; Kao et al., 2009), so we performed immunostaining in *RB:GFP* larvae at 3 dpf to asses SFK activity in distal somatosensory axons using an antibody that recognizes activated SFK (Y418). As previously reported, pSFK staining was highly enriched in skin cells and skin cell junctions (Yoo et al., 2011; Fig. 6*D*′). To specifically identify pSFK activity in somatosensory axons, we created a 3D axonal volume using the GFP+ axons of the *RB:GFP* transgenic and isolated solely the pSFK signal within axons (Fig. 6*D*″). We found that control larvae had notable pSFK signal within distal tail

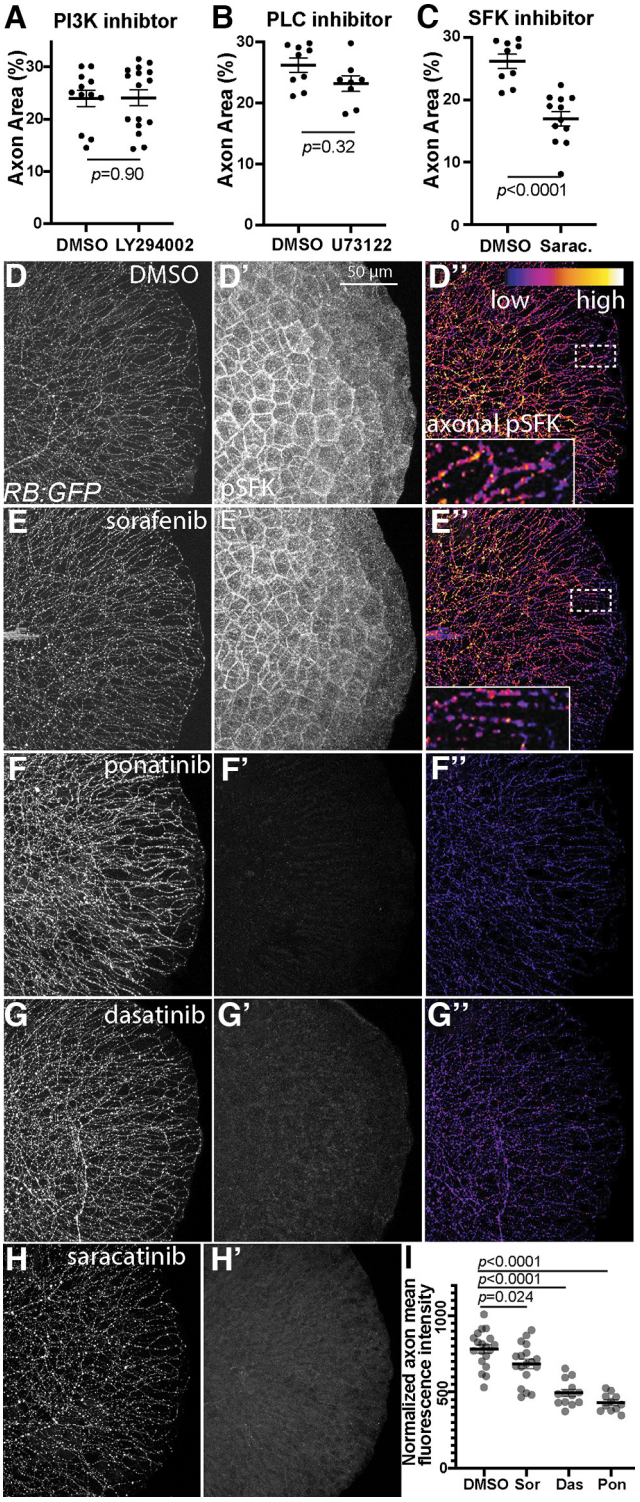

Figure 6. MKI treatment reduces axonal SFK activity. ***A–C***, Quantification of treatment of larvae treated with 25 μM LY294002, 0.75 μM PLC inhibitor U73122, or 30 μM saracatinib. Treatment with LY294002 or U73122 had no significant effect on axonal area but saracatinib did. Analyzed by unpaired *t* test. ***A***, DMSO = 26.1 ± 1.2% area, U73122 = 23.1 ± 1.3. ***B***, DMSO = 25.2 ± 1.9% area, LY294002 = 25.2 ± 1.8. ***C***, DMSO = 26.2 ± 1.2% area, saracatinib = 17 ± 1.2. ***D–H***, Lateral view of fixed tails from *RB:GFP* larvae treated with DMSO, sorafenib, ponatinib, dasatinib, or saracatinib for 7 h at 3 dpf. ***D'–H'***, Tail tissue pSFK immunostaining. ***D''–G''***, Axonal-only pSFK staining for DMSO-treated, sorafenib-treated, ponatinib-treated, and dasatinib-treated larvae. Sorafenib reduced axonal pSFK staining but did not notably affect other pSFK staining. Ponatinib, dasatinib, and saracatinib abolish nearly all pSFK staining throughout the tail tissue. Dashed white lines denote regions included in 4× inset. ***I***, Quantification of axonal pSFK staining following acute drug treatment, analyzed by one-way ANOVA with *post hoc* Dunnett's test versus DMSO controls. DMSO = 782 ± 27 A.U., sorafenib = 685 ± 31, ponatinib = 495 ± 23, dasatinib = 433 ± 17. Error bars represent SEM.

axons. Acute treatment with saracatinib (30 μM), an SFK inhibitor, induced a loss of pSFK signal throughout the tail tissue (Fig. 6*H'*), indicating that the pSFK antibody labeling is specific.

Because Src/SFKs are a potential axonal target of Kit signaling, we asked whether MKI-mediated inhibition of Kit disrupts pSFK activity in distal axons. Acute treatment for 7 h with sorafenib (7.5 μM), which does not directly inhibit SFKs, did not strongly affect the skin pSFK staining (Fig. 6*E'*) but induced significant reduction in distal axonal pSFK staining (Fig. 6*E''*). As expected, similar treatment with ponatinib (5 μM) or dasatinib (2 μM), both of which target Src/SFKs in addition to Kit, led to reduction of pSFK staining throughout the tail tissue (Fig. 6*F'*, *G'*), including significant loss of pSFK staining specifically in distal RB axons (Fig. 6*F''*,*G''*). These results indicate there is normally SFK activity in the distal axons at this time period and treatment with sorafenib, ponatinib, or dasatinib can significantly reduce this activity (Fig. 6*I*).

SFKs are downstream of Kitb and mediate cutaneous axon density

Our observations implied that SFKs may mediate Kitb signaling in RB axons. Indeed, we found a significant reduction in distal axonal pSFK staining in *kitb* mutants compared with WT (Fig. 7*A–C*). Moreover, SFK inhibition by saracatinib, a highly specific SFK inhibitor (Green et al., 2009), induced significant loss of RB axon density (Fig. 7*D*). Notably, treatment of *kitb* mutants with saracatinib did not exacerbate the loss of axon density (Fig. 7*D*), suggesting SFKs are a downstream target of Kit signaling that is critical for its role in regulating cutaneous sensory axon density. SFKs directly bind activated Kit receptor at two specific tyrosine phosphosites in mammals, Y567 and Y569 (Hong et al., 2004), which in turn activates SFKs. To test whether these phosphosites were required for Kitb's role in regulating RB axon density, we generated a Kitb receptor with phospho-dead mutations at both the zebrafish corresponding phosphosites (Y568F/Y570F) and attempted to suppress the axonal phenotype in *kitb* mutants. Unlike WT *kitb* mRNA, injection of $kit^{Y568F,Y570F}$ mRNA did not have any significant effects of axon density in *kitb* mutants at 3 dpf (Fig. 7*E*), suggesting Kit and SFK direct interaction is needed to regulate cutaneous axon density. Taken together, our results indicate inhibition of Kitb reduces axonal SFK activity that, in turn, disrupts normal cutaneous axon density and maintenance.

We next asked whether Kitlgb activation of Kitb induced changes in local axonal pSFK levels. Kitlgb was mosaically misexpressed in *RB:GFP* as described above and embryos were fixed at 3 dpf and immunostained for pSFK. RB axons in the RFP+, Kitlgb-expressing regions had significantly higher pSFK staining compared with adjacent RFP- regions, indicating local Kitb signaling increases SFK activity within axons (Fig. 7*F*,*G*, *kitlgb-p2a-mCherry-CAAX* positive = 1970 ± 202 MFI, negative = 1555 ± 179). This indicates Kitb signaling results in local increases in both axon density as well pSFK activity.

Kit inhibition similarly affects mammalian somatosensory neurons

MKIs are a major class of drugs used clinically for targeted cancer treatments. As with many small-molecule cancer treatments,

←

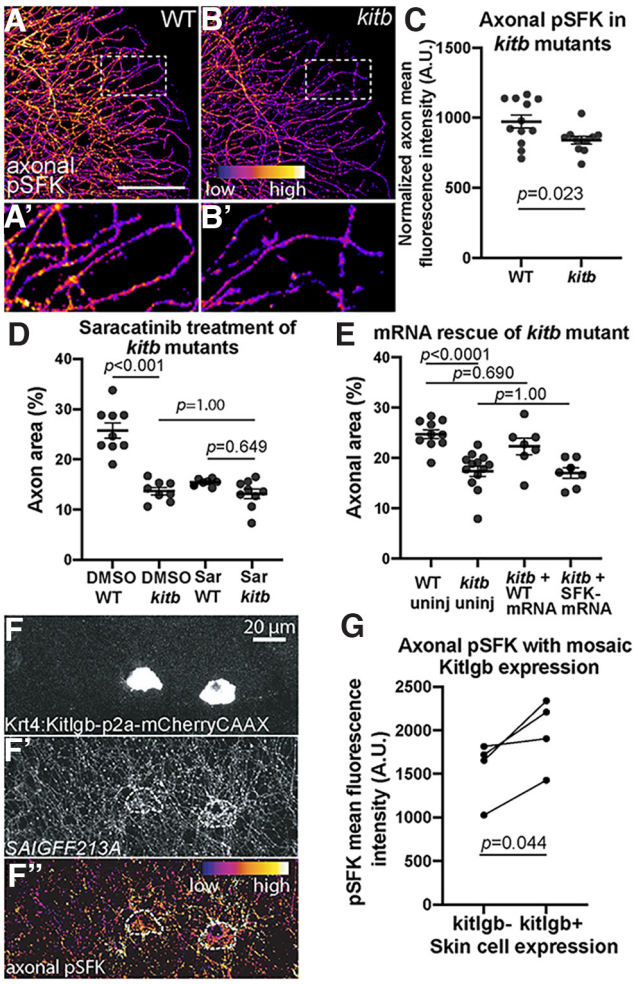

Figure 7. SFK activity regulates axon density downstream of Kitb. ***A***, ***B***, Axonal-only pSFK immunostaining for WT (***A***) and *kitb* (***B***) mutant 3 dpf larval tails. White dotted lines indicate regions of insets (***A'***, ***B'***) at 3× magnification. Scale bar: 50 μm. ***C***, Quantification of pSFK immunostaining intensity in distal larval tail axons. *Kitb* mutants have significantly reduced pSFK staining intensity compared with WT; WT = 920.0 ± 36.1 A.U. versus *kitb* mutant = 776.6 ± 36.6. ***D***, Quantification of saracatinib treatment of *kitb* mutants, analyzed by two-way ANOVA with *post hoc* Tukey's HSD test. DMSO WT = 25.8 ± 1.5%area, DMSO *kitb* = 13.7 ± 0.7, saracatinib WT = 15.4 ± 0.3, saracatinib *kitb* = 13.2 ± 0.9. ***E***, Quantification of axon density of *kitb* mutants injected with WT or $kitb^{Y568F,Y570F}$ mRNA ("SFK−"), analyzed by two-way ANOVA with *post hoc* Tukey's HSD test. WT uninjected = 24.7 ± 0.9% area, *kitb* mutant uninjected = 17.3 ± 1, *kitb* mutant + WT *kitb* mRNA = 22.3 ± 1.6, *kitb* mutant + Y568F/Y570F *kitb* mRNA ("kitb + SFK- mRNA") = 17.0 ± 1.1. ***F–F''***, Example of Krt4:Kitlgb-p2a-mCherryCAAX-injected 3 dpf larvae immunostained for pSFK. Axonal density and pSFK staining are increased in regions near Kitlgb expression (white dashes). ***G***, Quantification of mean axonal pSFK intensity in Kitlgb+ versus Kitlgb− regions within 3 dpf larvae, analyzed by paired *t* test. Error bars represent SEM.

MKIs can induce sensory neuropathies in a subset of patients. This includes sorafenib, ponatinib, and dasatinib, which induce peripheral neuropathies in 13%, 20%, and 31% of patients, respectively (Escudier et al., 2007; Cortes et al., 2010; Ariad, 2022). While the cellular bases of MKI-induced neuropathies are not understood, the pathophysiology of other peripheral neuropathic cancer compounds (e.g., taxanes, vinca alkaloids) has been described: distal sensory axon terminals retract and "die-back" with continued drug treatment, resulting in a reduction in cutaneous axon density (Pittenger et al., 2004; Devigili et al., 2008; Boyette-Davis et al., 2013; Fukuda et al., 2017). This cellular etiology is consistent with the *in vivo* effects we observe on cutaneous axons with MKI treatment. We thus asked whether these three drugs had a similar effect on growth and maintenance of somatosensory axons of Kit-responsive neurons in mammalian DRGs. Dissected embryonic mouse DRG explants cultured in media containing high levels of KITLG/SCF (but without other exogenously supplemented growth factors such as NGF) survive and produce a high proportion of c-Kit+ neurons (Hirata et al., 1993, 1995). DRGs were dissected (E15.5) and cultured for 24 h in media containing KITLG/SCF, then treated for 24 h with MKIs. Treatment of cultures with sorafenib, ponatinib, and dasatinib led to significantly shorter neurites and reduced axonal density compared with vehicle (Fig. 8*A–H*). These data suggest MKIs have a similar effect on mammalian somatosensory neurons as we observe in zebrafish.

Discussion

While extracellular signaling in sensory axon growth and pathfinding has been well studied, the role of receptor signaling pathways in maintaining established, functional axon terminals is less defined. We show that a major signaling pathway, c-Kit, is both necessary and sufficient to regulate cutaneous density of established sensory axon networks in a highly localized manner. Using *in vivo* analysis, we found that loss of Kit signaling induces retraction of distal sensory axon terminals, similar to the "dying-back" pathophysiology described with other neurotoxic drugs. Through pharmacological and genetic approaches, we identify SFKs as downstream targets of Kit that are critical for its function in mediating axon density and axon maintenance. Finally, we treated mammalian DRG explants with Kit inhibitors and found that the role of the Kit pathway in maintaining somatosensory axon density is evolutionarily conserved. Taken together, our data identify a novel role for Kit signaling in maintaining somatosensory axon density and lay the groundwork for further study into the neurobiological roles of the Kit-SFK signaling axis in axon development and health. Furthermore, our data provide new insight into the heretofore unstudied cellular mechanisms of MKI-induced sensory neuropathies and raise the possibility that disruption of Kit signaling may underlie some of these adverse effects.

Kit signaling mediates cutaneous innervation

c-Kit receptor is expressed in a subset of mammalian embryonic and adult somatosensory neurons, predominantly in unmyelinated, nociceptive c-fibers (Milenkovic et al., 2007; Sun et al., 2009; Usoskin et al., 2015). Expression of its ligand, SCF/KITLG, is detected in mouse embryonic and adult skin as well as larval zebrafish skin (Hultman et al., 2007). Mouse mutant studies found loss of Kit signaling may affect the identity/number of some DRG neurons, hamper DRG axon regeneration, and alter responses to certain stimuli (Lourenssen et al., 2000; Milenkovic et al., 2007; Sun et al., 2009). However, the exact role of Kit signaling and the relationship between the ligand/receptor expression pattern in somatosensory neuron development and function is still not fully elucidated. We find that *kitb* homozygous zebrafish mutants do not have significant loss of somatosensory neurons during development and *kitb* mutant cutaneous axons initially extend, branch, and reach the distal edge of the tail normally during early development. However, Kitb is necessary for maintaining axonal density beyond 36 hpf. Treatment of larvae well after the skin is fully innervated and axons are functional and elaborately arborized (3 dpf) with Kit inhibitors induces a similar reduction in axon density, confirming Kitb's role in the maintenance of axons within the skin.

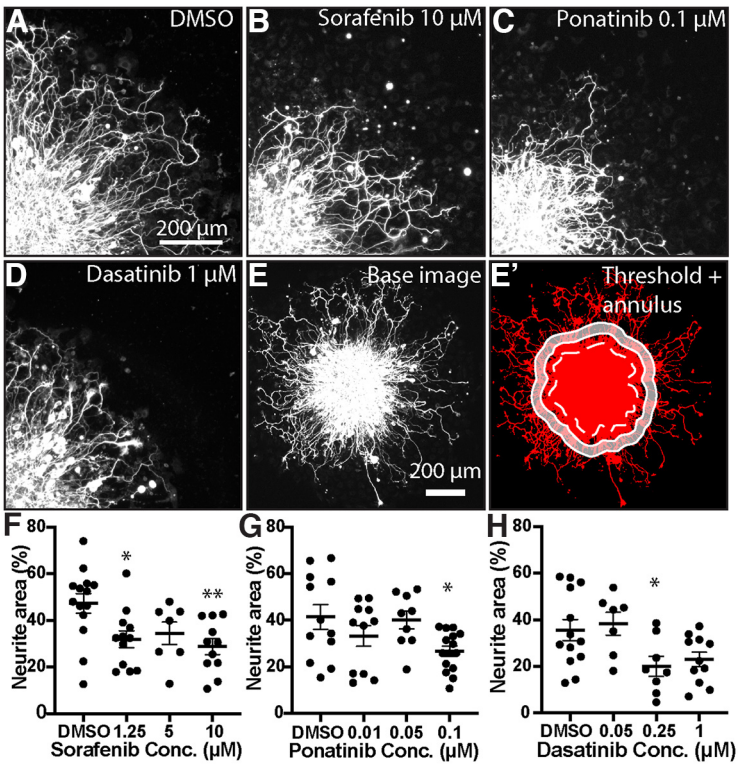

Figure 8. MKI treatment induces loss of neurite density in mammalian DRGs. ***A–D***, Single quadrant images of fixed DRG explants immunostained for βIII-Tubulin treated with vehicle or MKI compounds. MKI treatment led to shorter and less dense neurites. ***E***, ***E′***, Demonstration of neurite area analysis. Immunostained DRG explants were imaged (***E***), thresholded (***E′***, red), and then the explant core was identified (dotted white line) and a 50-μm-thick annulus (white shaded area) was created by drawing the inner and outer perimeter 50 and 100 μm from the edge of the explant core, respectively. ***F-H***, Quantification of neurite area, analyzed by one-way ANOVA with *post hoc* Dunnett's test. ***F***, Sorafenib: DMSO = 47.3 ± 4.2% area, 1.25 μM 32.0 ± 3.6, $p = 0.016$, 5 μM 34.5 ± 4.8, $p = 0.116$, 10 μM 28.8 ± 3.4, $p = 0.0039$. ***G***, Ponatinib: DMSO = 41.4 ± 5.3, 0.01 μM 33.3 ± 4.4, $p = 0.353$, 0.05 μM 40.1 ± 3.9, $p = 0.99$, 1 μM 26.8 ± 2.2 $p = 0.0215$. ***H***, Dasatinib: DMSO = 35.6 ± 4.5, 0.05 μM 38.4 ± 4.9, $p = 0.954$, 0.25 μM 20.0 ± 4.3, $p = 0.038$, 1 μM 23.0 ± 3.1, $p = 0.073$. Error bars represent SEM; $^*p < 0.05$, $^{**}p < 0.01$.

The RB neurons affected are polymodal, unmyelinated somatosensory neurons, similar to the population of DRG neurons that express c-Kit in mammalian models and are affected in *Kit* mutant mice. We also observe reductions in neurite density of SCF-grown mammalian DRG cultures treated with MKIs, suggesting that this neuronal response to Kit inhibition is conserved in mammalian somatosensory neurons. We find that local misexpression of Kitlgb induces a dramatic, highly localized increase in cutaneous axon density. The local increase in axonal density where Kitlgb is expressed in the skin falls off very rapidly, with significantly lower axonal density in directly adjacent areas and then axonal density reverting to normal levels beyond one-cell diameter. This suggests that Kitlgb misexpression is likely not "hijacking" other axons in the region to locally increase axonal density (at the expense of regional axonal density), but rather it is promoting local increases in axon density through impacting branching or axon size. These data indicate a critical role for Kit signaling in modulating cutaneous axon innervation and density.

The expression of Kit receptor in somatosensory neurons and the consistent expression of Kit ligand throughout the adult mouse and larval zebrafish skin suggests a constant role for Kit signaling in promoting and/or maintaining cutaneous axon innervation. We propose that the constant presence of Kit ligand maintains proper axonal arborization and density levels in the skin. We observe in zebrafish that somatosensory terminals are highly dynamic, and Kit signaling may promote axon terminal outgrowth that counteracts retraction or loss of arborization that may occur because of stochastic or directed dynamic terminal behavior. It may also be that SCF/Kit signaling promotes regeneration of fine somatosensory axon terminals. The cutaneous axon arbors of small-fiber, unmyelinated axons are intricate and superficial, yet these networks remain functional despite constant mechanical interaction with the environment. Furthermore, skin cells regularly turnover and axon terminals may need to dynamically adapt to local changes in tissue architecture. In these cases, these terminals would require consistent maintenance and regrowth and the presence of SCF throughout the skin may drive this via Kit signaling. In either case, we provide *in vivo* evidence that Kit signaling is an important regulator of cutaneous axon density and its specific effects on sensory axon behavior bear further study. Furthermore, Kit receptor or its downstream pathways may be candidates for future therapies attempting to ameliorate distal axonopathies including diabetes-induced and drug-induced peripheral neuropathies.

Kit inhibition induces axonal retraction

We observed treatment with three MKIs that strongly inhibit Kit induced significant reduction in cutaneous axon density of the tail. Although the larval caudal tail skin is fully-innervated with dense axon arbors at the time of drug treatment (72 hpf), it is possible that reduced axon density after drug treatment is because of defects in axon growth or arborization in the developing larva. However, in WT larvae we find no significant changes in distal axon density during the treatment/imaging window of 3–5 dpf, suggesting drug-induced changes in axon density are not because of growth inhibition. Furthermore, time-lapse imaging at the onset of drug treatment demonstrates individual axon terminals significantly retracting from their initial starting location rapidly following drug treatment. We conclude distal axonal retraction is a major cause of sorafenib, ponatinib, and dasatinib effects on cutaneous axon density. This drug-mediated effect is also strongly reminiscent of the "dying-back" effect of other peripheral neuropathic compounds (Fukuda et al., 2017).

SFK activity downstream of kit signaling

SFKs are one group of downstream effectors of activated Kit receptor. Src/SFKs regulate axon outgrowth and pathfinding in several vertebrate systems, including *Xenopus*, chick, and mouse spinal neurons (G. Liu et al., 2004; Robles et al., 2005; Tucker et al., 2008; Kao et al., 2009) and chick retinal neurons (Knöll and Drescher, 2004). SFKs also promote axon regeneration in peripheral sensory neurons in zebrafish DRGs, rat sciatic nerve, and *C. elegans* motor neurons (Zhao et al., 2003; Nichols and Smith, 2020; Sakai et al., 2021). In these contexts, SFKs affect axon growth and steering by regulating formation and localization of filopodia and lamellipodia within growth cones, affecting motility and direction (Robles et al., 2005; He et al., 2015). Although SFKs are an established target of activated Kit receptor, the two

have not been linked in the context of axon biology. Our results demonstrate axonal SFK activity is reduced by pharmacological or genetic loss of Kitb signaling and promoted locally through activation of Kitb. Additionally, SFK-binding phosphosites on Kitb are required for its role in regulating cutaneous somatosensory axon density. Finally, treatment with a pan-SFK inhibitor, saracatinib, induced similar losses of axon density compared with the other MKIs and did not further affect cutaneous axon density in *kitb* mutants. These results suggest that Kitb/SFK direct interaction is critical for its role in somatosensory axons and that modulation of Kitb signaling affects local axonal levels of pSFK.

Interestingly, inhibition of SFKs can ameliorate long-term peripheral neuropathic pain in rodent models. SFK activity in spinal neurons contributes to neuropathic pain by enhancing NMDA receptor activity (X.J. Liu et al., 2008). Long-term activation of SFKs in spinal microglia may also contribute to neuropathic pain from chronic formalin injection (Tan et al., 2012). In these cases, continuous SFK activation is associated with chronic neuropathic pain. However, SFK activity in growth cones and glia is also critical for peripheral axon regeneration (Zhao et al., 2003; Nichols and Smith, 2020). Based on our observations and the dynamic nature of these distal axon terminals, it is likely that SFK inhibition induces changes in axonal architecture by impeding its role as a promoter of axon outgrowth and regeneration. It is possible that short-term reduction of SFK activity contributes to axon retraction or failures in maintenance, but that long-term reduction of SFK activity may suppress neuropathic pain after the initial insult and/or regeneration is finished. SFKs, particularly Src, have functions in almost every cell type. Thus, systemic alteration of SFK activity can have many disruptive adverse effects. In contrast, modulating SFK activity through Kit signaling may offer a therapeutic opportunity to target SFKs in a cell-type specific manner to ameliorate the initial neurotoxic insult and also address SFK-mediated pain. Furthermore, local activation of Kit signaling in specific areas of the skin with topical compounds may provide a therapeutic strategy for specific distal neuropathies. Overall, these findings set the stage to elucidate the specific cellular and molecular mechanisms of Kit-SFK signaling in axon health and behavior and to explore how these pathways may interact with other disease states and peripheral neuropathic compounds.

References

Adnane L, Trail PA, Taylor I, Wilhelm SM (2006) Sorafenib (BAY 43-9006, Nexavar), a dual-action inhibitor that targets RAF/MEK/ERK pathway in tumor cells and tyrosine kinases VEGFR/PDGFR in tumor vasculature. Methods Enzymol 407:597–612.

Ariad (2022) ICLUSIG [package insert]. Cambridge: Ariad Pharmaceuticals, Inc.

Barkai O, Puig S, Lev S, Title B, Katz B, Eli-Berchoer L, Gutstein HB, Binshtok AM (2019) Platelet-derived growth factor activates nociceptive neurons by inhibiting M-current and contributes to inflammatory pain. Pain 160:1281–1296.

Boyette-Davis JA, Cata JP, Driver LC, Novy DM, Bruel BM, Mooring DL, Wendelschafer-Crabb G, Kennedy WR, Dougherty PM (2013) Persistent chemoneuropathy in patients receiving the plant alkaloids paclitaxel and vincristine. Cancer Chemother Pharmacol 71:619–626.

Cioni JM, Koppers M, Holt CE (2018) Molecular control of local translation in axon development and maintenance. Curr Opin Neurobiol 51:86–94.

Cirrincione AM, Pellegrini AD, Dominy JR, Benjamin ME, Utkina-Sosunova I, Lotti F, Jergova S, Sagen J, Rieger S (2020) Paclitaxel-induced peripheral neuropathy is caused by epidermal ROS and mitochondrial damage through conserved MMP-13 activation. Sci Rep 10:3970.

Cokus SJ, De La Torre M, Medina EF, Rasmussen JP, Ramirez-Gutierrez J, Sagasti A, Wang F (2019) Tissue-specific transcriptomes reveal gene expression trajectories in two maturing skin epithelial layers in zebrafish embryos. G3 (Bethesda) 9:3439–3452.

Cortes JE, Jones D, O'Brien S, Jabbour E, Ravandi F, Koller C, Borthakur G, Walker B, Zhao W, Shan J, Kantarjian H (2010) Results of dasatinib therapy in patients with early chronic-phase chronic myeloid leukemia. J Clin Oncol 28:398–404.

Devigili G, Tugnoli V, Penza P, Camozzi F, Lombardi R, Melli G, Broglio L, Granieri E, Lauria G (2008) The diagnostic criteria for small fibre neuropathy: from symptoms to neuropathology. Brain 131:1912–1925.

Drerup CM, Nechiporuk AV (2016) In vivo analysis of axonal transport in zebrafish. Methods Cell Biol 131:311–329.

Early JJ, Cole KL, Williamson JM, Swire M, Kamadurai H, Muskavitch M, Lyons DA (2018) An automated high-resolution in vivo screen in zebrafish to identify chemical regulators of myelination. Elife 7:e35136.

Escudier B, Eisen T, Stadler WM, Szczylik C, Oudard S, Siebels M, Negrier S, Chevreau C, Solska E, Desai AA, Rolland F, Demkow T, Hutson TE, Gore M, Freeman S, Schwartz B, Shan M, Simantov R, Bukowski RM; TARGET Study Group (2007) Sorafenib in advanced clear-cell renal-cell carcinoma. N Engl J Med 356:125–134.

Faucherre A, Nargeot J, Mangoni ME, Jopling C (2013) piezo2b regulates vertebrate light touch response. J Neurosci 33:17089–17094.

Fukuda Y, Li Y, Segal RA (2017) A mechanistic understanding of axon degeneration in chemotherapy-induced peripheral neuropathy. Front Neurosci 11:481.

García-Nafría J, Watson JF, Greger IH (2016) IVA cloning: a single-tube universal cloning system exploiting bacterial in vivo assembly. Sci Rep 6:27459.

Golden JP, Hoshi M, Nassar MA, Enomoto H, Wood JN, Milbrandt J, Gereau RW 4th, Johnson EM Jr, Jain S (2010) RET signaling is required for survival and normal function of nonpeptidergic nociceptors. J Neurosci 30:3983–3994.

Green TP, Fennell M, Whittaker R, Curwen J, Jacobs V, Allen J, Logie A, Hargreaves J, Hickinson DM, Wilkinson RW, Elvin P, Boyer B, Carragher N, Plé PA, Bermingham A, Holdgate GA, Ward WHJ, Hennequin LF, Davies BR, Costello GF (2009) Preclinical anticancer activity of the potent, oral Src inhibitor AZD0530. Mol Oncol 3:248–261.

Hall AK (2006) Rodent sensory neuron culture and analysis. Curr Protoc Neurosci Chapter3:Unit 3.19.

He Y, Ren Y, Wu B, Decourt B, Lee AC, Taylor A, Suter DM (2015) Src and cortactin promote lamellipodia protrusion and filopodia formation and stability in growth cones. Mol Biol Cell 26:3229–3244.

Hirata T, Morii E, Morimoto M, Kasugai T, Tsujimura T, Hirota S, Kanakura Y, Nomura S, Kitamura Y (1993) Stem cell factor induces outgrowth of c-kit-positive neurites and supports the survival of c-kit-positive neurons in dorsal root ganglia of mouse embryos. Development 119:49–56.

Hirata T, Kasugai T, Morii E, Hirota S, Nomura S, Fujisawa H, Kitamura Y (1995) Characterization of c-kit-positive neurons in the dorsal root ganglion of mouse. Brain Res Dev Brain Res 85:201–211.

Hong L, Munugalavadla V, Kapur R (2004) c-Kit-mediated overlapping and unique functional and biochemical outcomes via diverse signaling pathways. Mol Cell Biol 24:1401–1410.

Hultman KA, Bahary N, Zon LI, Johnson SL (2007) Gene Duplication of the zebrafish kit ligand and partitioning of melanocyte development functions to kit ligand a. PLoS Genet 3:e17.

Kao TJ, Palmesino E, Kania A (2009) SRC family kinases are required for limb trajectory selection by spinal motor axons. J Neurosci 29:5690–5700.

Kimmel CB, Ballard WW, Kimmel SR, Ullmann B, Schilling TF (1995) Stages of embryonic development of the zebrafish. Dev Dyn 203:253–310.

Knöll B, Drescher U (2004) Src family kinases are involved in EphA receptor-mediated retinal axon guidance. J Neurosci 24:6248–6257.

Kupari J, Usoskin D, Parisien M, Lou D, Hu Y, Fatt M, Lönnerberg P, Spångberg M, Eriksson B, Barkas N, Kharchenko PV, Loré K, Khoury S, Diatchenko L, Ernfors P (2021) Single cell transcriptomics of primate sensory neurons identifies cell types associated with chronic pain. Nat Commun 12:1510.

Kwan KM, Fujimoto E, Grabher C, Mangum BD, Hardy ME, Campbell DS, Parant JM, Yost HJ, Kanki JP, Chien CB (2007) The Tol2kit: a multisite

gateway-based construction kit for Tol2 transposon transgenesis constructs. Dev Dyn 236:3088–3099.
Lisse TS, Middleton LJ, Pellegrini AD, Martin PB, Spaulding EL, Lopes O, Brochu EA, Carter EV, Waldron A, Rieger S (2016) Paclitaxel-induced epithelial damage and ectopic MMP-13 expression promotes neurotoxicity in zebrafish. Proc Natl Acad Sci U S A 113:E2189–E2198.
Liu G, Beggs H, Jürgensen C, Park HT, Tang H, Gorski J, Jones KR, Reichardt LF, Wu J, Rao Y (2004) Netrin requires focal adhesion kinase and Src family kinases for axon outgrowth and attraction. Nat Neurosci 7:1222–1232.
Liu XJ, Gingrich JR, Vargas-Caballero M, Dong YN, Sengar A, Beggs S, Wang SH, Ding HK, Frankland PW, Salter MW (2008) Treatment of inflammatory and neuropathic pain by uncoupling Src from the NMDA receptor complex. Nat Med 14:1325–1332.
Lourenssen S, Motro B, Bernstein A, Diamond J (2000) Defects in sensory nerve numbers and growth in mutant Kit and Steel mice. Neuroreport 11:1159–1165.
Marcos-Gutiérrez CV, Wilson SW, Holder N, Pachnis V (1997) The zebrafish homologue of the ret receptor and its pattern of expression during embryogenesis. Oncogene 14:879–889.
Mariano V, Domínguez-Iturza N, Neukomm LJ, Bagni C (2018) Maintenance mechanisms of circuit-integrated axons. Curr Opin Neurobiol 53:162–173.
Mellgren EM, Johnson SL (2005) kitb, a second zebrafish ortholog of mouse Kit. Dev Genes Evol 215:470–477.
Metikala S, Casie Chetty S, Sumanas S (2021) Single-cell transcriptome analysis of the zebrafish embryonic trunk. PLoS One 16:e0254024.
Milenkovic N, Frahm C, Gassmann M, Griffel C, Erdmann B, Birchmeier C, Lewin GR, Garratt AN (2007) Nociceptive tuning by stem cell factor/c-Kit signaling. Neuron 56:893–906.
Mologni L, Redaelli S, Morandi A, Plaza-Menacho I, Gambacorti-Passerini C (2013) Ponatinib is a potent inhibitor of wild-type and drug-resistant gatekeeper mutant RET kinase. Mol Cell Endocrinol 377:1–6.
Muto A, Ohkura M, Kotani T, Higashijima S, Nakai J, Kawakami K (2011) Genetic visualization with an improved GCaMP calcium indicator reveals spatiotemporal activation of the spinal motor neurons in zebrafish. Proc Natl Acad Sci U S A 108:5425–5430.
Nichols EL, Smith CJ (2020) Functional regeneration of the sensory root via axonal invasion. Cell Rep 30:9–17.e3.
O'Hare T, et al. (2009) AP24534, a pan-BCR-ABL inhibitor for chronic myeloid leukemia, potently inhibits the T315I mutant and overcomes mutation-based resistance. Cancer Cell 16:401–412.
Ogino K, Hirata H (2018) Rohon-Beard neuron in zebrafish. In: Zebrafish, medaka, and other small fishes: new model animals in biology, medicine, and beyond (Hirata H and Iida A, eds), pp 59–81. Singapore: Springer Singapore.
Palanca AM, Lee SL, Yee LE, Joe-Wong C, Trinh l. A, Hiroyasu E, Husain M, Fraser SE, Pellegrini M, Sagasti A (2013) New transgenic reporters identify somatosensory neuron subtypes in larval zebrafish. Dev Neurobiol 73:152–167.
Pittenger GL, Ray M, Burcus NI, McNulty P, Basta B, Vinik AI (2004) Intraepidermal nerve fibers are indicators of small-fiber neuropathy in both diabetic and nondiabetic patients. Diabetes Care 27:1974–1979.
Plaza-Menacho I, Mologni L, Sala E, Gambacorti-Passerini C, Magee AI, Links TP, Hofstra RM, Barford D, Isacke CM (2007) Sorafenib functions to potently suppress RET tyrosine kinase activity by direct enzymatic inhibition and promoting RET lysosomal degradation independent of proteasomal targeting. J Biol Chem 282:29230–29240.
Rasmussen JP, Vo NT, Sagasti A (2018) Fish scales dictate the pattern of adult skin innervation and vascularization. Dev Cell 46:344–359.e4.
Rieger S, Sagasti A (2011) Hydrogen peroxide promotes injury-induced peripheral sensory axon regeneration in the zebrafish skin. PLoS Biol 9: e1000621.
Robles E, Woo S, Gomez TM (2005) Src-dependent tyrosine phosphorylation at the tips of growth cone filopodia promotes extension. J Neurosci 25:7669–7681.
Sakai Y, Tsunekawa M, Ohta K, Shimizu T, Pastuhov S, Hanafusa H, Hisamoto N, Matsumoto K (2021) The integrin signaling network promotes axon regeneration via the Src-Ephexin-RhoA GTPase signaling axis. J Neurosci 41:4754–4767.
Schindelin J, Arganda-Carreras I, Frise E, Kaynig V, Longair M, Pietzsch T, Preibisch S, Rueden C, Saalfeld S, Schmid B, Tinevez JY, White DJ, Hartenstein V, Eliceiri K, Tomancak P, Cardona A (2012) Fiji: an open-source platform for biological-image analysis. Nat Methods 9:676–682.
Shah AN, Davey CF, Whitebirch AC, Miller AC, Moens CB (2015) Rapid reverse genetic screening using CRISPR in zebrafish. Nat Methods 12:535–540.
Shah NP, Lee FY, Luo R, Jiang Y, Donker M, Akin C (2006) Dasatinib (BMS-354825) inhibits KITD816V, an imatinib-resistant activating mutation that triggers neoplastic growth in most patients with systemic mastocytosis. Blood 108:286–291.
Sun YG, Gracias NG, Drobish JK, Vasko MR, Gereau RW, Chen ZF (2009) The c-kit signaling pathway is involved in the development of persistent pain. Pain 144:178–186.
Takagi K, Okuda-Ashitaka E, Mabuchi T, Katano T, Ohnishi T, Matsumura S, Ohnaka M, Kaneko S, Abe T, Hirata T, Fujiwara S, Minami T, Ito S (2008) Involvement of stem cell factor and its receptor tyrosine kinase c-kit in pain regulation. Neuroscience 153:1278–1288.
Tan YH, Li K, Chen XY, Cao Y, Light AR, Fu KY (2012) Activation of Src family kinases in spinal microglia contributes to formalin-induced persistent pain state through p38 pathway. J Pain 13:1008–1015.
Tavares-Ferreira D, Shiers S, Ray PR, Wangzhou A, Jeevakumar V, Sankaranarayanan I, Cervantes A, Reese JC, Chamessian A, Copits BA, Dougherty PM, Gereau RW, Burton MD, Dussor G, Price TJ (2021) Spatial transcriptomics reveals unique molecular fingerprints of human nociceptors. bioRxiv 430065. doi: 10.1101/2021.02.06.430065.
Tucker BA, Rahimtula M, Mearow KM (2008) Src and FAK are key early signalling intermediates required for neurite growth in NGF-responsive adult DRG neurons. Cell Signal 20:241–257.
Tuttle A, Drerup CM, Marra M, McGraw H, Nechiporuk AV (2019) Retrograde Ret signaling controls sensory pioneer axon outgrowth. Elife 8:e46092.
Usoskin D, Furlan A, Islam S, Abdo H, Lönnerberg P, Lou D, Hjerling-Leffler J, Haeggström J, Kharchenko O, Kharchenko PV, Linnarsson S, Ernfors P (2015) Unbiased classification of sensory neuron types by large-scale single-cell RNA sequencing. Nat Neurosci 18:145–153.
Voytyuk O, Lennartsson J, Mogi A, Caruana G, Courtneidge S, Ashman LK, Rönnstrand L (2003) Src family kinases are involved in the differential signaling from two splice forms of c-Kit. J Biol Chem 278:9159–9166.
Westerfield M (2000) The zebrafish book: a guide for the laboratory use of zebrafish (Brachydanio rerio), Ed 4. Eugene: Institute of Neuroscience, University of Oregon.
Williams JA, Barrios A, Gatchalian C, Rubin L, Wilson SW, Holder N (2000) Programmed cell death in zebrafish rohon beard neurons is influenced by TrkC1/NT-3 signaling. Dev Biol 226:220–230.
Williams K, Ribera AB (2020) Long-lived zebrafish Rohon-Beard cells. Dev Biol 464:45–52.
Yao K, Ge W (2013) Spatial distribution and receptor specificity of zebrafish Kit system–evidence for a Kit-mediated bi-directional communication system in the preovulatory ovarian follicle. PLoS One 8:e56192.
Yoo SK, Starnes TW, Deng Q, Huttenlocher A (2011) Lyn is a redox sensor that mediates leukocyte wound attraction in vivo. Nature 480:109–112.
Zhao YL, Takagawa K, Oya T, Yang HF, Gao ZY, Kawaguchi M, Ishii Y, Sasaoka T, Owada K, Furuta I, Sasahara M (2003) Active Src expression is induced after rat peripheral nerve injury. Glia 42:184–193.